Reconstituted basement membrane enables airway epithelium modeling and nanoparticle toxicity testing

Elrade Rofaani, Boxin Huang, Feng Liang, Juan Peng, Yong Chen

Reconstituted basement membrane enables airway epithelium modeling and nanoparticle toxicity testing

Elrade Rofaani [a,b], Boxin Huang [a], Feng Liang [a], Juan Peng [a*] and Yong Chen [a*]

[a] École Normale Supérieure-PSL Research University,

Sorbonne Université, CNRS UMR 8640 PASTEUR, Paris, 75005, France

[b] National Research and Innovation Agency, Jakarta, 10340, Indonesia

[*]e-mail: yong.chen@ens.psl.eu and juan.wang@ens.psl.eu

A short statistical summary of the article includes:

- 7448 words
- 6 figures
- 4 figures of supplement

Reconstituted basement membrane enables airway epithelium modeling and nanoparticle toxicity testing

Elrade Rofaani [a,b], Boxin Huang [a], Feng Liang [a], Juan Peng [a*] and Yong Chen [a*]

[a] École Normale Supérieure-PSL Research University,

Sorbonne Université, CNRS UMR 8640 PASTEUR, Paris, 75005, France

[b] National Research and Innovation Agency, Jakarta, 10340, Indonesia

[*]e-mail: yong.chen@ens.psl.eu and juan.wang@ens.psl.eu

Abstract

Basement membrane (BM) acts as a sheet-like extracellular matrix to support and promote the formation of epithelial and endothelial cell layers. The in-vitro reconstruction of the BM is however not easy due to its ultrathin membrane features. This difficult is overcome by self-assembling type IV collagen and laminin in the porous areas of a monolayer of crosslinked gelatin nanofibers deposited on a honeycomb microframe. Herein, a method is presented to generate airway epithelium by using such an artificial basement membrane (ABM) and human-induced pluripotent stem cells (hiPSCs). Bipolar primordial lung progenitors are firstly induced from hiPSCs and then replated on the ABM for differentiation toward matured airway epithelium under submerged and air-liquid interface culture conditions. As result, a pseudostratified airway epithelium consisting of several cell types is achieved, showing remarkable apical secretion of MUC5AC proteins and clear advantages over other types of substrates. As a proof of concept, the derived epithelium is used for toxicity test of cadmium telluride (CdTe) nanoparticles (NPs), demonstrating the applicability of ABM-based assays involving hiPSC-derived epithelial cells. based assays.

Keywords: hiPSCs, airway epithelium, basement membrane, nanoparticles

1. Introduction

The respiratory tract is covered with a continuous layer of airway epithelial cells including columnar club, ciliated, goblet, and basal cells. These cells are specialized for exocrine production, mucociliary clearance, mucus secretion, and renewing of the cells, respectively [1]. Structurally, the airway epithelial cells are organized into a pseudostratified cell layer on a basement membrane (BM) composed of collagen IV, laminin, and proteoglycans [2]. Together, this airway epithelium plays a critical role in maintaining air transportation to and from the alveoli of the lungs and protecting against air-borne pathogens or micro-dusts [2]. Damage or disorder of the airway epithelium may cause respiratory-related diseases such as chronic obstructive pulmonary disease and lower respiratory tract infections [1,2]. To understand the mechanism of airway diseases and test the safety and efficiency of new therapies, animals are often used as models of human disease but they cannot recapitulate the full spectrum of human pathophysiology and/or immune response. About 80% of drug candidates who succeeded in preclinical tests with rodents fail to effectively treat human diseases during clinical trials [3]. In-vitro models rely on immortalized cell lines such as Calu-3 which allow generating adherent monolayers with tight/adherens junction proteins (ZO-1 and E-Cadherins) [4]. However, due to their cancer origin, they can result in different phenotypes but lack multicellular types. In-vitro models using primary cells are useful but they are limited in cell viability and lack reproducibility [5]. In this regard, in-vitro models based on the differentiation of stem cells should be more reliable than other approaches [6]. In particular, human induced pluripotent stem cells (hiPSCs) are capable of self-renewing over many generations [7] and differentiation into different cell types [8], thus holding a high application potential for disease modeling, drug discovery, and regenerative medicine involving airway epithelial cells.

Previously, hiPSCs were used to produce airway epithelial cells [9-14] and airway organoids [15-17]. Interestingly, the formation of organoids begins with an embedment with a gel containing extracellular matrix (ECM) proteins, which promote organogenesis. With the size increase of the organoid, the organized cell layer counteracts the ECM in the gel which led to a progressive accumulation of the ECM to form a BM like structure [18]. Moreover, the generated airway organoids are inherently of multicellular types and suitable for early stage developmental studies and disease modeling. However, cells in the organoids are not exposed to air and cannot be easily analyzed by using techniques such as transepithelial electrical resistance (TEER). In contrast, airway epithelial cells differentiated on a membrane can be used directly for TEER analyses under air-liquid interface (ALI) conditions. The problem is that the

previous studies were mostly based on the use of micro-engineered membranes such as transwell inserts, patterned membranes with through holes, or nanofiber mats [19-24]. Compared with the natural BM, these membranes are not continuous and thin enough in terms of biological relevance. Ideally, an artificial basement membrane (ABM) needs recapitulate the main features of natural BM morphologically and physiochemically. This is particularly important for the formation of a hiPSC-derived epithelium, due to the strong dependence of stem cell differentiation on extracellular matrices [25] and the maintenance of the epithelial integrity and homeostasis [26]. Based on such an approach, advanced airway models may be established for disease modeling and nanoparticle toxicity studies [27-29].

Herein, we report a method to generate airway epithelium by differentiating hiPSCs-derived bipolar primordial lung progenitors (PLP) on a new type of ABM obtained by self-assembling type IV collagen and laminin with a monolayer of crosslinked gelatin nanofibers as backbone and a patterned honeycomb microframe for handling. While the hiPSC-PLPs are the first cells specified to a lung epithelial cell fate within the foregut that can be self-renewed and differentiated into either airway or alveolar cells, the ABM does not only provide a mechanical support for ALI culture but also specific signaling molecules as well as a high permeability for enhanced nutrient uptake and metabolite clearance [30]. Similar devices without self-assembling BM proteins were previously used to support the differentiation of hiPSCs toward cardiomyocytes [31] and neurons [32,33] and A549 cell monocouches [34]. In this work, we focus on the formation of functional pseudostratified airway epithelium involving goblet, ciliated, and basal cells. The advantage of using ABM in ariway differentiation is shown by comaprison to glass slide and nanofiber-covered glass (NFG). Notably, an enhanced apical secretion of MUC5AC proteins was observed with the ABM supported epithelium due to differentiation of hiPSC-PLPs on a more compliant substrate. Besides, we also demonstrate the reliability of the fabricated epithelium for toxicity test of cadmium telluride (CdTe) nanoparticles (NPs).

2. Materials and methods

2.1. Fabrication of artificial basement membrane

The ABM device was fabricated by using lithography, electrospinning, chemical crosslinking, and self-assembling techniques. Briefly, a honeycomb structure of 400-μm hole size, 50-μm linewidth, and 50-μm thickness were defined in a SU-8 photoresist (Microchem, France) by photolithography. This pattern was sequentially replicated into polydimethylsiloxane (PDMS, Eleco-EFD, France) by casting and polyethylene glycol

diacrylate (PEGDA) by vacuum-assisted UV-curing. Afterward, the final replica (frame) was coated by 10 nm Au and gelatin nanofibers were electrospun. Gelatin (10 wt%) (#61890, Sigma-Aldrich, France) was dissolved in a mixed solution of acetic acid, ethyl acetate (#270989, Sigma-Aldrich, France), and deionized (DI) water at a volume ratio of 21:14:10. The nanofibers were deposited at a distance of 10 cm and voltage 11 kV for 5 min, controlled with a high voltage supply (Heinzinger, Germany), a syringe pump (#789100B, Kd Scientific, USA) at a feeding rate of 0.2 mL/h. After electrospinning, gelatin nanofibers were dried in a desiccator overnight and cross-linked in a 0.2 M mixture of 1-ethyl-3-(3-dimethylaminopropyl) carbodiimide (EDC, #6383, Sigma-Aldrich, France) and N-hydroxysuccinimide (NHS) (#130672, Sigma-Aldrich, France) in ethanol for 4 h. After crosslinking, a monolayer of gelatin nanofibers was obtained. To eliminate remaining toxic chemicals, samples were rinsed in 99.5% ethanol three times, dried in a vacuum overnight, and finally submerged in sterilized DI water overnight.

The fabricated monolayer of nanofibers was used as backbone for self-assembling BM proteins in the pores of the monolayer. A 50 μL solution composed of 0.1% (w/v) type IV collagen (#C7521, Sigma-Aldrich, France) in water containing 0.1 M acetic acid and 2% (v/v) laminin (#L2020, Sigma-Aldrich, France) was pipetted on the nanofiber system. After dehydration at 37°C for 3–5 h, a reconstituted BM or ABM, contains an ultrathin layer of collagen IV-laminin mixture, could be obtained. To evaluate the general properties of the ABM, measurements of scanning electron microscopy, contact angle, deflection [34,35], and Darcy permeability [36] were conducted and an ABM handling device for ALI culture has been realized by machining or three-dimensional (3D) printing. For comparison, nanofibers were also deposited on the glass using a gold-coated 13-mm diameter cover glass in a similar manner as described above and the resulted samples were referred as nanofibers on glass (NFG).

2.2. Production of matured airway epithelial cells

hiPSCs (episomal line, Life Technologies, France) were cultured and maintained in complete E8 Flex medium (#A2858501, Gibco) with a 1:100 diluted vitronectin (#A27940, Life Technologies)-coated culture dish and incubated at 37˚C with 5% CO_2 condition. The medium was changed every two days until cells grew to 70–80% confluence. The cells were harvested with a solution of Dulbecco's Phosphate Buffered Saline (DPBS, #14190-094, Gibco) with 0.5 mM ethylene diamine tetra-acetic acid (EDTA, #15575-038, Life Technologies).

Following the previous protocols, hiPSCs were differentiated into airway progenitor cells (APCs) and then matured airway epithelial cells (AECs) by using different types of substrates,

all coated with 1% of Geltrex. Overall, hiPSCs were derived sequentially to (i) definitive endoderm (DE) (6 days), (ii) anterior foregut endoderm (AFE) (2 days), (iii) bipotential primordial lung progenitors (PLPs) (7 days), (iv) airway progenitor cells (APC) (6-10 days), and (v) matured AECs (17 days).

DE induction: Prior to induction, hiPSCs were cultured in a dish with 50% confluence. The induction medium of serum-free RPMI1640 (#21875034, Gibco) containing 1% glutamine, 1% penicillin-streptomycin or pens-strep (#15140122, Gibco) and 1% non-essential amino acid (NEAA) or B-27 (#17504-044, Gibco) and 0.1% ascorbic acid (#A4403, Sigma-Aldrich), was prepared with high concentration of Activin A (100 ng/mL) (#78001.1, Stemcell Technologies) and 1 μM CHIR-99021 (#SML1046, Sigma-Aldrich). The cells were induced in this medium for 6 days to generate DE or to undergo a gastrulation process. The medium was changed every two days.

AFE patterning: From day 6 to 8, cells were treated with serum-free IMDM medium (#12440-053, Gibco) containing 1% glutamax, 1% pens-strep, 1% B-27 and 0.1% ascorbic acid, as a serum-free IMDM medium, then supplemented with 10 μM SB-431452 (#HB3555, Hellobio) and 1.5 μM dorsomorphine or DSM (#P5499, Sigma-Aldrich).

Generation of PLP: From day 8 to 15, cells were cultured in a serum-free IMDM medium containing 3 μM CHIR-99021, growth factor of 10 ng/mL KGF or FGF-7 (#251-KG, R&D System), 10 ng/mL BMP4 (#78211, Stemcell Technologies) and 0.0625 μM retinoic acid or RA (#R2625, Sigma-Aldrich).

APC derivation: at day 15, PLPs were digested with tryplE (#12605-010, Life Technologies) for 5 min and seeded in diluted 1:100 geltrex- (#A1413302, Life Technologies) coated ABM, NFG and glass. The cells were resuspended in a serum-free IMDM medium containing a factor of airway epithelial cells maturation, 10 ng/mL FGF18 (#78041.1, Stemcell Technologies) and a growth factor for epithelium proliferation, 10 ng/mL KGF for the APC derivation. The medium was changed every two days until day 21.

From APCs to AECs: From day 22 to 39, APCs were cultured in a serum-free IMDM medium containing 10 ng/mL FGF18, 10 ng/mL KGF, and a cocktail molecule, composed of 0.1 mM isobutylmethylxanthine, iBMX (#I5879, Sigma-Aldrich); 0.1 mM 8-bromo-cAMP (#D0627, Sigma-Aldrich), 25 ng/mL dexamethasone (#4902, Sigma-Aldrich), which are usually referred to as DCI. The ABM with cells was mounted in homemade transwell support (Boyden chamber) and placed in a 6 well plate (#734-2323, VWR). The ABM-inserted Boyden chamber was used for ALI culture. The cells were taken place in the top compartment of Boyden chamber. After one day of culture, the medium in the top compartment was removed gently and

washed by DPBS 3x, leaving the apical surface of the cells exposed to air (in an atmosphere of 5% CO_2 at 37°C). Afterward, the culture was continued and the medium in the low compartment was changed every two days.

2.3. Immunostaining microscopy

Cells were rinsed with DPBS and fixed with 4% paraformaldehyde (#P6148, Sigma-Aldrich) for 15 min. Samples were permeabilized with 0.5% Triton X-100 (#HFH10, Life Technologies) for 20 min and saturated with DPBS supplemented with 0.1% Triton X-100 and 3% BSA (#A9056, Sigma-Aldrich) for 2 h at room temperature. DPBS was contained 0.1% v/v Tween20 (#P1379, Sigma-Aldrich). Afterward, staining was performed with primary antibodies overnight at 4°C. On day 21, all progenitors were stained by primary unconjugated antibody NKX2.1 (#MA5-13961, Invitrogen) and ZO-1 (#40-2200, Invitrogen), followed by the secondary antibody Alexa Fluor 488 and 633 (#A-11008 and #A-21086, Invitrogen). At day 39 or maturation step, airways cells were stained by primary unconjugated antibody MUC5AC (#MA5-12178, Invitrogen) and ZO-1, followed by the secondary antibody Alexa Fluor 488 and 555 (#A-11008 and #A-31572, Invitrogen). Primary cilia are stained with acetylated α-tubulin (#T7451-100UL, Sigma-Aldrich) and Actin (#R37112, Invitrogen) were used for labeling ciliated cells. All samples were observed with LSM Zeiss 710 confocal microscope (Zeiss, France). Images were collected as TIF files and analyzed with the software ImageJ.

2.4. Nanoparticle exposure on maturated AECs

COOH-functionalized CdTe-NPs (#777986, Sigma-Aldrich) were used for toxicity assays with matured airway cells. These NPs were 3-11 nm in size, soluble and negatively charged. To achieve a homogenous distribution of the cells, the ABM was mounted on a homemade PDMS chamber of 7 mm diameter and 1 x 10^5 airway epithelial cells were seeded and incubated for 24 h, before the co-culture with CdTe NPs. Before confocal imaging, the cells were fixed and immune-stained with primary unconjugated antibody ZO-1, followed by the secondary antibody Alexa Fluor 488. CdTe NP is red fluorescent while nuclei were stained by DAPI (blue).

2.5. Statistical analysis

The data, between groups, are shown as the mean ± SEM (Standard Error of the Mean) from at least three samples were statistically analyzed using ANOVA with performing Tukey test using the software GraphPad Prism software (GraphPad, USA). Significance was set to $^{*}P< 0.05$, ** $P< 0.01$, and *** $P< 0.001$.

3. Results

3.1. Characterization of the reconstituted basement membrane

To generate the functional airway epithelium, we followed a general differentiation strategy of hiPSCs [12] but an ABM as a cell culture support. The fabrication of the ABM was straightforward, involving lithography, electrospinning, and self-assembling techniques (Fig. 1a). The fabricated ABM device was characterized by means of scanning electron microscopy (SEM) and quantitative measurements of contact angle, stiffness and permeability of the membrane. Fig. 1b shows phase-contrast image of a crosslinked monolayer of nanofibers (MNF) with a patterned honeycomb compartment from which a porosity of ~30% could be deduced. Fig. 1c shows SEM image of an ABM obtained after BM protein deposition with an MNF backbone. Here, the periodic hexagonal structure is 500 µm in pitch and 50 µm in thickness and width. Typically, the fabricated ABM has a thickness of ~200 nm under optimal processing conditions. The contact angle measurements showed that the ABM has a wetting character comparable to that of glass slide but different from that of the MNF (Fig. 1d, Fig. S1). By measuring the deflection of the membrane under pressure in a similar way as described in [34] but with the help of an additional PDMS thin layer [35], an effective Young's modulus of the ABM, 4.9 MPa, could be deduced. This value is compared to the effective Young's modulus of the MNF obtained with same method so that the stiffness of ABM could be mainly due to its nanofiber backbone. By measuring the flow rate of DI water crossing a sample of MNF or ABM as a function of applied pressure, the Darcy permeability of the sample, 2.4×10^{-15} m² and 7.2×10^{-15} m², could be determined respectively [36]. Such permeability is at least ten times larger than that of commonly used etched ion track membranes, due to very small thickness of the MNF and the ABM samples.

3.2. Generation of airway progenitor cells from hiPSCs

The PLPs are capable to be differentiated into either proximal (airway) or distal (alveolar) lung cells. Following a reported protocol, we firstly derived hiPSCs into PLPs [12] (Fig.2, Fig. S2). From day 0 to 6, hiPSC colonies were induced into DE with Activin A and CHIR-99021. From day 7 to 8, DE was patterned into AFE by inhibiting bone morphogenic protein (BMP) and TGF-β signaling pathways. From day 9 to 15, the cells became bipotential primordial lung progenitors and cyst-like features were observed in addition to the epithelial-like cells. On day 15, we replated the PLPs on different types of culture substrates of Geltrex-coated ABM, NFG, and glass to generate airway progenitors. After one day of replating (day 16), cells formed a

monolayer by sub-merged culture. At the end of progenitor development on day 21, the epithelial-like formation was observed on the ABM and NFG substrates, while only a limited number of cells were observed on the glass substrate (Fig. S3), indicating the suitability of nanofibers' morphology.

The immunofluorescence images of the sample with progenitor cells on ABM showed high-level expressions of NKX2.1 (homeodomain-containing transcription factor) and ZO-1 (Zonula occludens-1) proteins (Fig. 3a). Here, the ventral marker NKX2.1 is a nuclear transcription factor and is actively involved in committing progenitor of lung fate. Tight junction (TJ) marker ZO-1 is typically related to the development of epithelial cell polarization for providing an established permeability barrier for ion/molecules diffusion [36]. By counting the number of nuclei, the cell density could be calculated and compared, confirming significant differences in cell spreading and proliferation growing on the three different substrates (Fig. 3c). Finally, the percentage of NKX2.1 positive cell was higher than the previously reported ones [13-15] and the expression levels of NKX2.1 and ZO-1 proteins of the cells on ABM were significantly higher than that on glass and NFG (Fig. 3d, 3e). Morphologically, the airway progenitors on ABM were organized in dense monolayer with larger heights (Fig. 3b, 3f). In addition, an intact cellular monolayer on ABM was established by special ZO-1 proteins on the apical surface, suggesting a controlled epithelial-cell polarization and the formation of morphologically distinct apical domains during cell development. These apical domains allow bidirectional signaling that receives signals from the cell interior and regulates in turn the cell behavior.

3.3. Differentiation of airway progenitor cells to airway epithelial cells

On day 22, the airway progenitors on ABM were placed in a homemade Boyden chamber to differentiate them into airway epithelial cells under submerged and ALI culture conditions. A serum-free maturation medium containing a mixture of growth factors FGF18 [38] and KGF and DCI [39] was used for airway epithelial development over 17 days. On day 39, some of the cells showed high levels of expression of MUC5AC proteins (Fig. 4a). Similar cells were also found in the immunostaining images of the cells on NFG. The cross-sectional views of the cell layers indicated that these cells have typical features of airway epithelial goblet cells, showing a vertically elongated cell shape and secretion into the apical compartment of the MUC5AC proteins, as marked by white arrowheads [40] (Fig. 4b). In addition to the goblet cells, at least two other cells types could be observed, one with nuclei on the same level of the MUC5AC proteins and another one with nuclei sited on the ABM, indicated by orange and yellow arrowheads, respectively (Fig. 4b). These cells could be attributed to ciliated cells and basal

cells within a pseudostratified epithelium. Indeed, ciliated cells could be observed by immunostaining of acetylated α-tubulin, showing marked primary cilia lined on the apical surface of the cells (see below). Furthermore, the cell boundaries marked by ZO-1 could be seen but they fluctuated due to the pseudostratified epithelial structure. Concerning the basal cells located immediately above the basement membrane, they are capable of self-renewal and differentiation into both ciliated and goblet cells so that they are fundamentally important for maintenance and regeneration of the airway epithelial barrier [1,2]. Therefore, the observation of the three types of cells on ABM suggest that the differentiating cells were more efficiently organized on the ABM than on NFG. Statistically, the cell density on ABM is about 1.5-folds more than that on NFG, due to the high proliferation rate (Fig. 4c). Nevertheless, the percentage of MUC5AC-positive cells on the ABM and NFG remained unchanged (Fig. 4d). However, the cells on ABM expressed twice more MUC5AC proteins than that on NFG (Fig. 4e), suggesting that both behaviors and functions of the cells were regulated by the underlying substrate and ABM does not only promote the formation of pseudostratified epithelium but also high-level expression of airway specific proteins of the cells. Finally, due to high proliferation rate and low substrate stiffness, large epithelial tensile forces could be generated which may deform the underlying ABM, all depending on the initial cell seeding density.

Primary cilia stained by acetylated α-tubulin are dynamic structures of microtubule and transiently present during the differentiation of airway epithelial cells. They are used for mucociliary clearance, which is the primary innate defense of the lung [40]. Fig. 5 shows immunofluorescence images of the cells on the ABM, indicating a high-level expression of the acetylated α-tubulin proteins. The top view image (left) revealed a random distribution of elongated cilia with a number of distinct spots where the ciliated cells located. The cross-section view images (XZ and YZ) show that the primary cilia expression was located at the center of the apical surface as indicated more clearly by the white arrows, in agreement with the previous observation [40].

3.4. Exposure of airway epithelial cells to CdTe nanoparticles

The functional test of the fabricated airway epithelium was performed with COOH functionalized CdTe nanoparticles (NPs). While bulk CdTe is currently used to make thin-film solar cells, the CdTe NPs are attractive for many applications such as biological probing and solid-state lighting due to their strong and stable fluorescence. The bulk CdTe has low acute inhalation, oral, and aquatic toxicity, but the CdTe NPs may be harmful due to cellular uptake and translocation of the airway epithelium. Our results showed that after 24 h the CdTe NPs

could be inhaled by the cells or aggreged on the cell surfaces (Fig. 6a). On day 2, the cell layer was damaged at a dosage of 7.5 µg/mL and even completely destroyed at higher dosages. Fig. 6b and 6c show the immunofluorescence images of the cells incubated with a culture medium with or without containing 7.5 µg/mL CdTe NPs for 24 h. Without CdTe NPs, the airway cells were regularly distributed on the ABM with clear cell boundaries marked by ZO-1 proteins (Fig. 6b). With CdTe NPs, no more cell boundary could be clearly observed even though some residues of the ZO-1 proteins could still be identified, indicating the toxicity of NPs. The effect of cellular up-taken and nucleus nearby localization of the CdTe NPs could also be observed (Fig. 6c).

4. Discussion

The airway epithelium consists of cellular and acellular components which are both important for the integrity and homeostasis of the tissue. Any in-vitro model will be subjected to a variety of assays but the most important is the establishment of a reliable development strategy. In our case, hiPSC derived airway cells are used which can be obtained/processed more easily than primary cells and advantageous over immortalized cell lines. For example, poor P450 enzyme activity was detected in Calu-3 cell lines due to low expression and non-inducibility of CYP1A1 and CYP2B cytochromes and the absence of functional CYP3A4. This greatly affects its metabolic response and limits its potential ability to screen potential drug candidates and formulations [4]. In contrast, hiPSC derived cells generally have molecular phenotype similar to primary adult cells of either healthy donors or patient specific diseases [9-14]. On the other hand, the most of the previous in-vitro airway models were based on conventional culture plate [9] or engineered porous membrane made of polycarbonate, polyester, PDMS, or nanofibers [10-14,19-24]. Compared to the ABM, these membranes are much thick, stiff, inhomogeneous and less permeable. These intrinsic features do not change after the surface coating of the appropriate biomolecules, which is clearly a drawback for the generation of airway epithelium. hiPSC-derived airway organoids are generally formed in gel instead of at ALI [15-17]. However, the hiPSC-derived organoids can be dissociated into single cells and then replated on a membrane for ALI culture, which may enhance the expression of airway-specific proteins and stimulate ciliation, polarization, and barrier functions [13,14]. Nevertheless, ABM is preferable for replating since it does not only allow an early setting of the epithelium but also promote the self-organization of the pseudostratified epithelial layers during PLP differentiation and airway barrier maturation due to its relative low stiffness and

high permeability. Indeed, we observed that after replating, fewer cells remained on the glass due to poor formation of the epithelia layers caused by stressed cytoskeleton.

It is known that the performance of adherent cell culture and in particular hiPSC differentiation depends critically on the stiffness compliance with the underlying substrate [43-46]. The stiffness of the ABM is due mainly to the nanofiber backbone. To estimate the in-plan stiffness of the backbone, we may consider a hexagonal lattice made of nanofiber segments of diameter *a* and length *l*. Then, the effective in-plane and out-plane Young's modulus of the lattice can be obtained analytically, $E=\frac{4}{\sqrt{3}}E_s(\frac{a}{l})^3$ and $\frac{2}{\sqrt{3}}E_s(\frac{a}{l})$, where E_s is the bulk Young's modulus of the material [47]. For a typical ratio of a/l = 0.1, the effective in-plane Young's modulus is ~4.9 kPa, which is three orders of magnitude smaller than E_s. Such a Young's modulus is comparable to that of lung tissues [48]. This means that the epithelial generated forces could be sufficient large to interplay with the underlying ABM. Therefore, a high PLP seeding density may result in an over increased cell number so that an epithelial folding due to cell proliferation and low stiffness of the membrane. In practice, the cell seeding density and the replating time after induction can be controlled to achieve a relative flat epithelium.

Our results showed that the PLPs cells could be more efficiently proliferated and differentiated on ABM than on glass and nanofiber-covered glass, showing up-regulated expression of NKX2.1 and TJ proteins. Here, NKX2.1+ cells were analyzed as intermediates to functional airway epithelial cells. We noticed that in the previous studies the NKX2.1+ cells were mostly obtained in a dish before replating on a membrane and that a mesenchymal layer could be spontaneously generated underneath the NKX2.1+ cells due to unsuitable stiffness and permeability of the plastic membranes. After replating and maturation, the presence of the mesenchymal cells in the airway epithelium [12] might be problematic for the accuracy of TEER measurements. One solution was to sort NKX2.1+ cells and generate firstly "epithelial-only" airway organoids and then the airway epithelial cells of different types [12]. However, the signaling of the cells in their putative niche before replating should not be ignored [49]. In this regard, a higher percentage of NKX2.1+ cells achieved with ABM is beneficial for the airway epithelium formation. Moreover, these cells under ALI culture conditions led to a pseudostratified epithelium consisting of several cell types with a high-level expression of MUC5AC proteins. We believe that the high permeability of the ABM also promotes the formation of the pseudostratified layer since it facilitates both nutrient up taking and metabolite clearance, in addition to the signalling of type IV collagen and laminin ligands cell adhesion and proliferation. Both may greatly reduce the occurrence of feeder layers even through

mesodermal elements could be induced in our differentiation protocol [9]. We would also like to mention that in such a protocol, the growth factor FGF-18 was used to promote Clara cell generation [10] which is necessary for the proximal airway formation [38] and that KGF (FGF7) belongs to the fibroblast growth factor family generally involved in lung tissue formation [42]. Thus, this protocol is relatively simple but efficient to generate airway cells of multiple types which could be improved with the ABM. Overall, the differentiation and maturation processes last 39 days, which is comparable to other differentiation protocols [9-12] but significantly less than those involving organoid formation and dissociated cell replating [13,14].

Finally, the observed attachment of CdTe NPs to the airway epithelium could be attributed to the interaction between negative charges of the NPs and positive charge of cells' plasma membrane [50,51]. It is known that goblet cells secrete mucus to form a viscoelastic layer on the surface of the outer plasma membrane of the cells which can trap foreign objects for the translocation involving cellular uptake and tissue surface clearance [52]. Previous studies have shown that hydrophilic NPs could be more easily translocated through the surfactant film compared to hydrophobic NPs [53-55]. In our case, the toxicity of the CdTe NPs was mainly due to the high dosages. Statistically, the NPs at high doses have a high probability to be up-taken and translocated on the plasma membrane of the cell, causing excessive inflammation to result in either extrinsic or intrinsic apoptotic processes. Altogether, the opposite charge interaction on the cell membrane, the surfactant trap of goblet cells, and the presence of high dose NPs led to damage of the airway epithelium, indicating the toxicity of the CdTe NPs. Clearly, a more systematic investigation is needed to study the responses of the airway epithelium to CdTe and other types of NPs by considering, for example, more relevant dosages, real-time barrier monitoring, high throughput, and microfluidic techniques.

5. Conclusion

We reported a method for airway epithelium modelling by using reconstituted or artificial BM and hiPSCs. This method relied on the self-organization of differentiating progenitors which could be enhanced by the underlying ABM under submerged and ALI culture conditions. While the intermediate airway progenitors highly expressed ventral protein markers (NKX2.1) and TJ protein (ZO-1), the goblet cells of matured airway epithelium highly expressed MUC5AC proteins. Due to the high proliferation rate of the progenitors and strong BM attachment of the cells, the resulting epithelium showed pseudostratified organization involving goblet, ciliated, and basal cells. Finally, the produced airway epithelium was used for toxicity

testing with CdTe nanoparticles. Our results showed that the airway epithelium was heavily damaged due to surface deposition and clustering of the nanoparticles.

Author contributions

E.R. performed the device preparation, characterization, and hiPSC differentiation experiments, B.H. and L.F aided in device making and cell culturing. J.P. and Y.C. was involved in planning and data analyses. All authors discussed the results and commented on the manuscript.

Aknowledgment

ER was granted by Indonesia Endowment Fund for Education, Ministry of Finance of The Republic of Indonesia (LPDP).This work has received support from French National Research Agency (ANR-17-CE09-0017, ANR-10-IDEX-0001-02 PSL, and ANR-10-LABX-31), Région Ile-de-France (DIM-ELICIT), and PSL-valorization (program pre-maturation). The authors would like to thank DR. Yong He for kindly providing the PDMS cell seeding chamber.

Declarations

Conflicts of Interest. No conflict of interest exists for the authors.

References

[1] J.D. Davis,T.P. Wypych, Cellular and functional heterogeneity of the airway epithelium. Mucosal Immunol 14 (2021) 978–990.https://doi.org/10.1038/s41385-020-00370-7.

[2] A. Tam, S. Wadsworth, D. Dorscheid, S.F. Man, D.D. Sin. The airway epithelium: more than just a structural barrier. Ther Adv Respir Dis. 5(2011) 255-73. https://doi.org/10.1177/1753465810396539.

[3] H.S. Warren, R.G. Tompkins, L.L. Moldawer, J. Seok, W. Xu, M.N. Mindrinos, R. V. Maier, W. Xiao, R.W. Davis, Mice are not men, Proc. Natl. Acad. Sci. U. S. A. 112 (2015) E345. https://doi.org/10.1073/pnas.1414857111

[4] K.A. Foster, M.L. Avery, M. Yazdanian, K.L. Audus, Characterization of the Calu-3 cell line as a tool to screen pulmonary drug delivery, Int. J. Pharm. 208 (2000) 1–11. https://doi.org/10.1016/S0378-5173(00)00452-X.

[5] A.A. Pezzulo, T.D. Starner, T.E. Scheetz, G.L Traver, A.E.Tilley, B.G.Harvey, R.G. Crystal, P.D. Jr. McCray, J. Zabner, The air-liquid interface and use of primary cell cultures are important to recapitulate the transcriptional profile of in vivo airway epithelia. Am J Physiol Lung Cell Mol Physiol. 300 (2011)L25-31. https://doi.org/10.1152/ajplung.00256.2010.

[6] A.J. Miller, J.R. Spence, In vitro models to study human lung development, disease and homeostasis, Physiology. 32 (2017) 246–260. http://doi.org/10.1152/physiol.00041.2016

[7] K. Takahashi, K. Tanabe, M. Ohnuki, M. Narita, T. Ichisaka, K. Tomoda, S. Yamanaka, Induction of Pluripotent Stem Cells from Adult Human Fibroblasts by Defined Factors, Cell. 131 (2007) 861–872. https://doi.org/10.1016/j.cell.2007.11.019.

[8] G. Liu, B.T. David, M. Trawczynski, et al. Advances in Pluripotent Stem Cells: History, Mechanisms, Technologies, and Applications. Stem Cell Rev and Rep 16 (2020) 3–32. https://doi.org/10.1007/s12015-019-09935-x.

[9] S.X.L. Huang, M.N. Islam, J. O'Neill, Z. Hu, Y.G. Yang, Y.W. Chen, M. Mumau, M.D. Green, G. Vunjak-Novakovic, J. Bhattacharya, H.W. Snoeck, Efficient generation of lung and airway epithelial cells from human pluripotent stem cells, Nat. Biotechnol. 32 (2014) 84–91. https://doi.org/10.1038/nbt.2754.

[10] A.P. Wong, C.E. Bear, S. Chin, P. Pasceri, T.O. Thompson, L.J. Huan, F. Ratjen, J. Ellis, J. Rossant, Directed differentiation of human pluripotent stem cells into mature airway epithelia expressing functional CFTR protein, Nat. Biotechnol. 30 (2012) 876–882. https://doi.org/10.1038/nbt.2328.

[11] A.L. Firth, C.T. Dargitz, S.J. Qualls, T. Menon, R. Wright, O. Singer, F.H. Gage, A. Khanna, I.M. Verma, Generation of multiciliated cells in functional airway epithelia from human induced pluripotent stem cells, Proc. Natl. Acad. Sci. U. S. A. 111 (2014). https://doi.org/10.1073/pnas.1403470111.

[12] K.B. McCauley, F. Hawkins, M. Serra, D.C. Thomas, A. Jacob, D.N. Kotton, Efficient Derivation of Functional Human Airway Epithelium from Pluripotent Stem Cells via Temporal Regulation of Wnt Signaling, Cell Stem Cell. 20 (2017) 844-857.e6. https://doi.org/10.1016/j.stem.2017.03.001.

[13] F. Hawkins, S. Suzuki, M. Lou Beermann, C. Barillà, R. Wang, C. Villacorta-Martin, A. Berical, J.C. Jean, J. Le Suer, C. Simone-Roach, Y. Tang, T. Schlaeger, A. Crane, S. Huang, S. Randell, A. Rab, E. Sorscher, A. Horani, S. Brody, B. Davis, D. Kotton, Derivation of Airway Basal Stem Cells from Human Pluripotent Stem Cells, (2020). https://doi.org/10.1101/2020.02.21.959395.

[14] K.M. Abo, Liang Ma, Taylor Matte, Jessie Huang, Konstantinos D. Alysandratos,

Rhiannon B. Werder, Aditya Mithal, Mary Lou Beermann, Jonathan Lindstrom-Vautrin, Gustavo Mostoslavsky, Laertis Ikonomou, Darrell N. Kotton, Finn Hawkins, Andrew Wilson, and Carlos V, Human iPSC-derived alveolar and airway epithelial cells can be cultured at air-liquid interface and express SARS-CoV-2 host factors, BioRxiV. (2020). http://doi.org/10.1101/2020.06.03.132639.

[15] Q. Tan, K.M.Choi, D.Sicard, D.J. Tschumperlin, Human airway organoid engineering as a step toward lung regeneration and disease modeling, Biomaterials,113 (2017) 118-132, ttps://doi.org/10.1016/j.biomaterials.2016.10.046

[16] J. Zhou, C. Li, N. Sachs, M. C. Chiu, B. H. Wong, H. Chu, et al. Differentiated human airway organoids to assess infectivity of emerging influenza virus, Proc Natl Acad. Sci U S A.115 (2018) 6822-6827; http://doi.org/10.1073/pnas.1806308115

[17] N. Sachs, A. Papaspyropoulos, D.D. Zomer-van Ommen, I. Heo, L. Böttinger, D. Klay, F. Weeber, G. Huelsz-Prince, N. Iakobachvili, G.D. Amatngalim, J. Ligt, A. Hoeck, N. Proost, M.C. Viveen, A. Lyubimova, L. Teeven, S. Derakhshan, J. Korving, H. Begthel, J.F. Dekkers, K. Kumawat, E. Ramos, M.F. Oosterhout, G.J. Offerhaus, D.J. Wiener, E.P. Olimpio, K.K. Dijkstra, E.F. Smit, M. Linden, S. Jaksani, M. Ven, J. Jonkers, A.C. Rios, E.E. Voest, C.H. Moorsel, C.K. Ent, E. Cuppen, A. Oudenaarden, F.E. Coenjaerts, L. Meyaard, L.J. Bont, P.J. Peters, S.J. Tans, J.S. Zon, S.F. Boj, R.G. Vries, J.M. Beekman, H. Clevers, Long-term expanding human airway organoids for disease modeling, EMBO J. 38 (2019) 1–20. https://doi.org/10.15252/embj.2018100300.

[18] M. Hofer, M.P. Lutolf, Engineering organoids, Nat. Rev. Mater. 6 (2021) 402–420. https://doi.org/10.1038/s41578-021-00279-y.

[19] K.H. Benam, R. Novak, J. Nawroth, M. Hirano-Kobayashi, T.C. Ferrante, Y. Choe, R. Prantil-Baun, J.C. Weaver, A. Bahinski, K.K. Parker, D.E. Ingber, Matched-Comparative Modeling of Normal and Diseased Human Airway Responses Using a Microengineered Breathing Lung Chip, Cell Syst. 3 (2016) 456-466.e4. https://doi.org/10.1016/j.cels.2016.10.003.

[20] Y. Zhu, A. Chidekel, T.H. Shaffer, Cultured Human Airway Epithelial Cells (Calu-3): A Model of Human Respiratory Function, Structure, and Inflammatory Responses, Crit. Care Res. Pract. 2010 (2010) 1–8. https://doi.org/10.1155/2010/394578.

[21] D. Huh, B.D. Matthews, A. Mammoto, M. Montoya-Zavala, H.T. Hsin, D.E. Ingber, Reconstituting organ-level lung functions on a chip. Science. 2010 Jun 25;328(5986):1662-8. https://doi.org/10.1126/science.1188302

[22] A.O. Stucki, J.D. Stucki, S.R.R. Hall, M. Felder, Y. Mermoud, R.A. Schmid, T. Geiser, O.T. Guenat, A lung-on-a-chip array with an integrated bio-inspired respiration mechanism, Lab Chip. 15 (2015) 1302–1310. https://doi.org/10.1039/c4lc01252f.

[23] T. Bluhmki, S. Bitzer, J.A. Gindele, E. Schruf, T. Kiechle, M. Webster, J. Schymeinsky, R. Ries, F. Gantner, D. Bischoff, J. Garnett, R. Heilker, Development of a miniaturized 96-Transwell air–liquid interface human small airway epithelial model, Sci. Rep. 10 (2020) 1–14. https://doi.org/10.1038/s41598-020-69948-2.

[24] D. Kim, S. Eom, S.P.Park, et al. A collagen gel-coated, aligned nanofiber membrane for enhanced endothelial barrier function. Sci Rep 9 (2019) 14915 https://doi.org/10.1038/s41598-019-51560-8

[25] L.R. Smith, S. Cho, D.E. Discher, Stem cell differentiation is regulated by extracellular matrix mechanics, Physiology. 33 (2018) 16–25. https://doi.org/10.1152/physiol.00026.2017.

[26] R. Jayadev, D.R. Sherwood, Basement membranes. Curr Biol. 27 (2017):R207-R211. https://doi.org/10.1016/j.cub.2017.02.006.

[27] S. Dekali, C. Gamez, T. Kortulewski, K. Blazy, P. Rat, G. Lacroix, Assessment of an in

vitro model of pulmonary barrier to study the translocation of nanoparticles, Toxicol. Reports. 1 (2014) 157–171. https://doi.org/10.1016/j.toxrep.2014.03.003.
[28] J.E. Nichols, J.A. Niles, S.P. Vega, J. Cortiella, Novel in vitro respiratory models to study lung development, physiology, pathology and toxicology, Stem Cell Res. Ther. 4 (2013) 4–8. https://doi.org/10.1186/scrt368.
[29] S. Dwivedi, M. A. Siddiqui, N. N. Farshori, M. Ahamed, J. Musarrat, Abdulaziz A. Al-Khedhairy, Synthesis, characterization and toxicological evaluation of iron oxide nanoparticles in human lung alveolar epithelial cells, Colloids and Surfaces B: Biointerfaces,122,2014,209-215, http:// doi.org/10.1016/j.colsurfb.2014.06.064
[30] E. Rofaani, J. Peng, L. Wang, Y. He, B. Huang, Y. Chen, Fabrication of ultrathin artificial basement membrane for epithelial cell culture, Microelectron. Eng. 232 (2020) 111407. https://doi.org/10.1016/j.mee.2020.111407.
[31] Y. Tang, L. Liu, J. Li, L. Yu, L. Wang, J. Shi, Y. Chen, Induction and differentiation of human induced pluripotent stem cells into functional cardiomyocytes on a compartmented monolayer of gelatin nanofibers, Nanoscale. 8 (2016) 14530–14540. https://doi.org/10.1039/c6nr04545f.
[32] Y. Tang, L. Liu, J. Li, L. Yu, F.P.U. Severino, L. Wang, J. Shi, X. Tu, V. Torre, Y. Chen, Effective motor neuron differentiation of hiPSCs on a patch made of crosslinked monolayer gelatin nanofibers, J. Mater. Chem. B. 4 (2016) 3305–3312. https://doi.org/10.1039/c6tb00351f.
[33] B.X. Huang, J. Peng, X.C. Huang, F. Liang, L. Wang, J. Shi, A. Yamada and Y. Chen, Generation of Interconnected Neural Clusters in Multiscale Scaffolds from Human-Induced Pluripotent Stem Cells, ACS Appl. Mater. Interfaces 13 (2021) 55939–55952. https://doi.org/10.1021/acsami.1c18465
[34] M. Radiom, Y. He, J. Peng-Wang, A. Baeza-Squiban, J.F. Berret, Y. Chen, Alveolar mimics with periodic strain and its effect on the cell layer formation, Biotechnol. Bioeng. 117 (2020) 2827–2841. https://doi.org/10.1002/bit.27458.
[35] Y. He, E. Rofaani, X. Huang, X., B. Huang, F. Liang, L. Wang, J. Shi, J. Peng, Y. Chen, Generation of Alveolar Epithelium Using Reconstituted Basement Membrane and hiPSC-Derived Organoids. Adv. Healthcare Mater. 2022, 2101972. https://doi.org/10.1002/adhm.202101972
[36] F. Linag, X. Huang, J. Peng, H. Luo, J. Shi, L. Wang, C. Aime, Y. Chen, A microfluidic system for rapid determination of Darcy permeability: from filtration membrane with patterned micro-holes to artificial basement membranes, to be published
[37] A. Hartsock, W.J. Nelson, Adherens and tight junctions: Structure, function and connections to the actin cytoskeleton, Biochim. Biophys. Acta - Biomembr. 1778 (2008) 660–669. https://doi.org/10.1016/j.bbamem.2007.07.012.
[38] J.A. Whitsett, J.C. Clark, L. Picard, J.W. Tichelaar, S.E. Wert, N. Itoh, A.K.T. Perl, M.T. Stahlman, Fibroblast growth factor 18 influences proximal programming during lung morphogenesis, J. Biol. Chem. 277 (2002) 22743–22749. https://doi.org/10.1074/jbc.M202253200.
[39] L.W. Gonzales, S.H. Guttentag, K.C. Wade, A.D. Postle, P.L. Ballard, Differentiation of human pulmonary type II cells in vitro by glucocorticoid plus cAMP, Am. J. Physiol. - Lung Cell. Mol. Physiol. 283 (2002) 940–951. https://doi.org/10.1152/ajplung.00127.2002.
[40] M.C. Rose, J.A. Voynow, Respiratory tract mucin genes and mucin glycoproteins in health and disease, Physiol. Rev. 86 (2006) 245–278. https://doi.org/10.1152/physrev.00010.2005.
[41] S.F Mao, A. S. Shah, T.O. Moninger, L. S. Ostedgaard, L. Lu, X.X.Tang, I.

M. Thornell, L. R. Reznikov, S. E. Ernst, P. H. Karp, P. Tan, S. Keshavjee, M. H. Abou Alaiwa, M. J. Welsh, PNAS, 115 (2018) 1370-1375; http://dio.org:10.1073/pnas.1719177115
[42] D. Lebeche, S. Malpel, W. V. Cardoso, Fibroblast growth factor interactions in the developing lung, Mech. Dev. 86 (1999) 125–136. https://doi.org/10.1016/S0925-4773(99)00124-0.
[43] P. Srivastava, A.K. Kilian, Micro-Engineered Models of Development Using Induced Pluripotent Stem Cells, Frontiers in Bioengineering and Biotechnology, 7 (2019) 357
[44] B. Wang, J. Shi, J. Wei, X. Tu, Y. Chen, Fabrication of elastomer pillar arrays with elasticity gradient for cell migration, elongation and patterning, Biofabrication. 11 (2019). https://doi.org/10.1088/1758-5090/ab21b3.
[45] B. Wang, X. Tu, J. Wei, L. Wang, Y. Chen, Substrate elasticity dependent colony formation and cardiac differentiation of human induced pluripotent stem cells, Biofabrication. 11 (2019). https://doi.org/10.1088/1758-5090/aae0a5.
[46] S. Li, F.P.U. Severino, J. Ban, L. Wang, G. Pinato, V. Torre, Y. Chen, Improved neuron culture using scaffolds made of three-dimensional PDMS micro-lattices, Biomed. Mater. 13 (2018). https://doi.org/10.1088/1748-605X/aaa777.
[47] L.J. Gibson, M.F. Ashby, Cellular Solids: Structure and Properties, 2 Ed., Cambridge Univ. Press. Cambridge. (1997). https://doi.org/10.1017/CBO9781139878326.
[48] C.F. Guimarães, L. Gasperini, A.P. Marques, R.L. Reis, The stiffness of living tissues and its implications for tissue engineering, Nat. Rev. Mater. 5 (2020) 351–370. https://doi.org/10.1038/s41578-019-0169-1.
[49] M.L. Donne, A.J. Lechner, and J.R Rock, Evidence for lung epithelial stem cell niches. BMC Dev Biol 15 (2015) , 32. https://doi.org/10.1186/s12861-015-0082-9
[50] K.C. Nguyen, W.G. Willmore, A.F. Tayabali, Cadmium telluride quantum dots cause oxidative stress leading to extrinsic and intrinsic apoptosis in hepatocellular carcinoma HepG2 cells, Toxicology. 306 (2013) 114–123. https://doi.org/10.1016/j.tox.2013.02.010.
[51] L.S. Ostedgaard, T.O. Moninger, J.D. McMenimen, N.M. Sawin, C.P. Parker, I.M. Thornell, L.S. Powers, N.D. Gansemer, D.C. Bouzek, D.P. Cook, D.K. Meyerholz, M.H.A. Alaiwa, D.A. Stoltz, M.J. Welsh, Gel-forming mucins form distinct morphologic structures in airways, Proc. Natl. Acad. Sci. U. S. A. 114 (2017) 6842–6847. https://doi.org/10.1073/pnas.1703228114.
[52] H.S. Choi, Y. Ashitate, J.H. Lee, S.H. Kim, A. Matsui, N. Insin, M.G. Bawendi, M. Semmler-Behnke, J. V. Frangioni, A. Tsuda, Rapid translocation of nanoparticles from the lung airspaces to the body, Nat. Biotechnol. 28 (2010) 1300–1303. https://doi.org/10.1038/nbt.1696.
[53] S. Mura, H. Hillaireau, J. Nicolas, S. Kerdine-Römer, B. Le Droumaguet, C. Deloménie, V. Nicolas, M. Pallardy, N. Tsapis, E. Fattal, Biodegradable nanoparticles meet the bronchial airway barrier: How surface properties affect their interaction with mucus and epithelial cells, Biomacromolecules. 12 (2011) 4136–4143. https://doi.org/10.1021/bm201226x.
[54] G. Hu, B. Jiao, X. Shi, R.P. Valle, Q. Fan, Y.Y. Zuo, Physicochemical properties of nanoparticles regulate translocation across pulmonary surfactant monolayer and formation of lipoprotein corona, ACS Nano. 7 (2013) 10525–10533. https://doi.org/10.1021/nn4054683.
[55] M. Kendall, P. Ding, R.M. MacKay, R. Deb, Z. McKenzie, K. Kendall, J. Madsen, H. Clark, Surfactant protein D (SP-D) alters cellular uptake of particles and nanoparticles, Nanotoxicology. 7 (2013) 963–973. https://doi.org/10.3109/17435390.2012.689880.

Figure caption:

Fig. 1. Fabrication and characterization of culture patch with artificial basement membrane. (a) Schematic diagram of the fabrication involving UV lithography patterning, nanofiber electrospinning, and protein self-assembling techniques. (b) Phase-contrast image of crosslinked monolayer of nanofibers (MNF) with a patterned honeycomb compartment. (c) SEM image of the device after BM protein self-assembling, showing artificial basement membrane (ABM) and embedded MNF backbone. (d) Contact angles of DI water, PBS, and culture medium on different types of substrates.

Fig. 2. Differentiation of hiPSCs toward matured airway epithelium. (a) Stepwise protocol passing through bipotential primordial lung progenitors and airway progenitors. (b) Schematic diagram of different culture configurations (adherent, sub-merged, and air-liquid interface culture). A photograph of the ABM mounting device is also shown. Scale bar: 50 μm.

Fig. 3. Immunofluorescence images of hiPSC-derived airway progenitors on ABM, nanofiber-covered glass (NFG), and glass. (a) Expression of NKX2.1 (green) and ZO-1 (red) proteins of the cells. Cell nuclei were stained with DAPI (blue). (b) Cross-sectional view (XZ) of NKX2.1, ZO-1, and DAPI. Statistical analyses of cell density (c), NKX2.1 (d) and ZO-1 (e) expression levels, and nuclei height (f) of the cells on three types of substrates. Scale bar: 50 μm.

Fig. 4. Immunofluorescence images and statistic data of matured airway epithelial cells. (a) Expression of MUC5AC (green) and ZO-1(red) proteins of the cells on ABM and nanofiber-covered glass (NFG). Cell nuclei were stained with DAPI (blue). (b) Cross-sectional view (XZ) of MUC5AC, ZO-1, and DAPI of the cells, showing typical pseudostratified organization where nuclei of neighboring cells appear at different levels. White arrowheads indicate MUC5AC+ cells (goblet cells), orange and yellow arrowheads indicate ciliated and basal cells. Statistical analyses of cell density on days 21 and 39 (c), percentage of MUC5AC+ cells (d), and MUC5AC expression levels of the cells on NFG and ABM (e). Scale bars: 50 μm.

Fig. 5. Immunofluorescence images of matured airway epithelial cells, after staining with acetylated tubulin (green), actin (red), and DAPI (blue). Left: Elongated cilia and location of ciliated cells (green spots). Right: The cross-section view images (XZ and YZ) show that the cilia expression of cells was located above nuclei and pointed by white arrows. Scale bar: 20 μm.

Fig. 6. Toxicity test of CdTe nanoparticles with hiPSC derived airway epithelium (patch). (a) Phase-contrast images of an airway patch incubated with CdTe-NP at a concentration of 7.5 µg/ml. Scale bar: 200 µm. Immunofluorescence images of the airway cells before (b) and after (c) incubation with 7.5 µg/ml CdTe-NP for 24h. ZO-1 proteins were stained green, CdTe in red, and cell nuclei in blue. Scale bars: 50 µm.

Figure 1

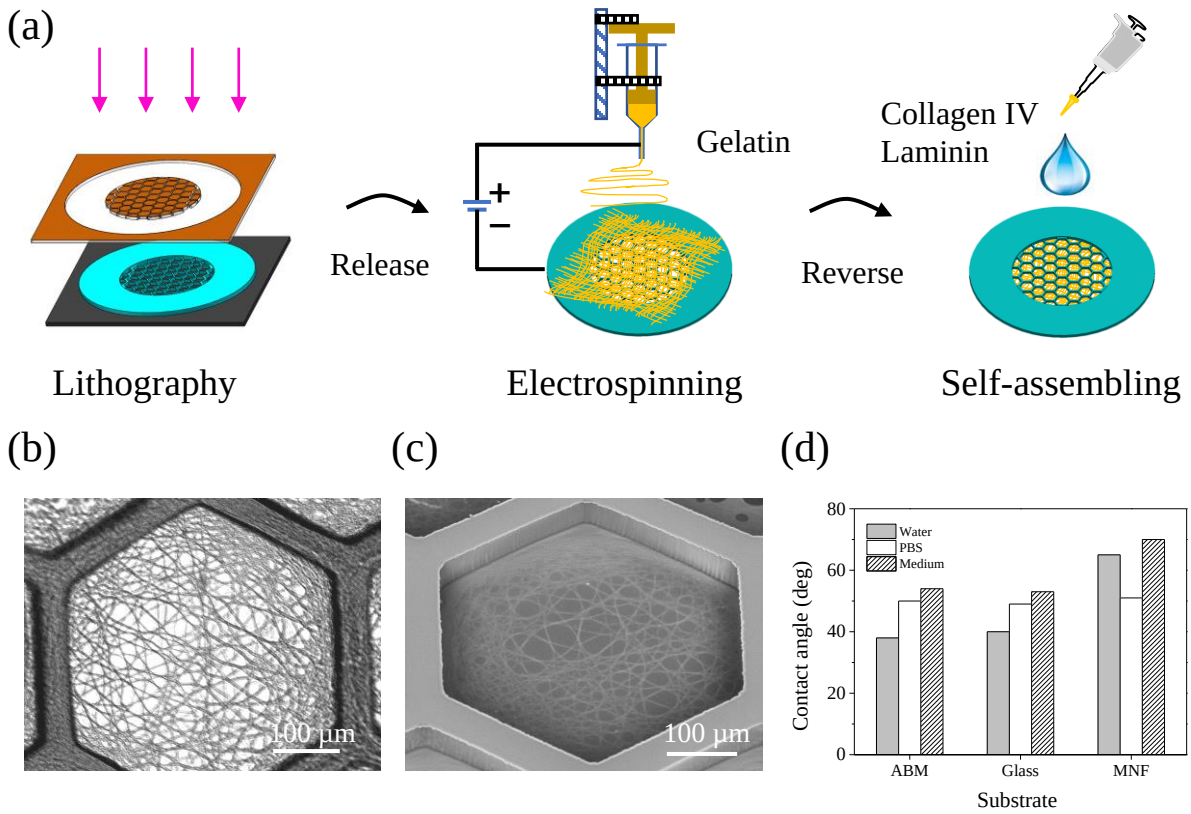
(a)
Release
Gelatin
Reverse
Collagen IV
Laminin
Lithography
Electrospinning
Self-assembling
(b)
(c)
(d)
100 μm
100 μm
Water
PBS
Medium
Contact angle (deg)
0
20
40
60
80
ABM
Glass
MNF
Substrate

Figure 2

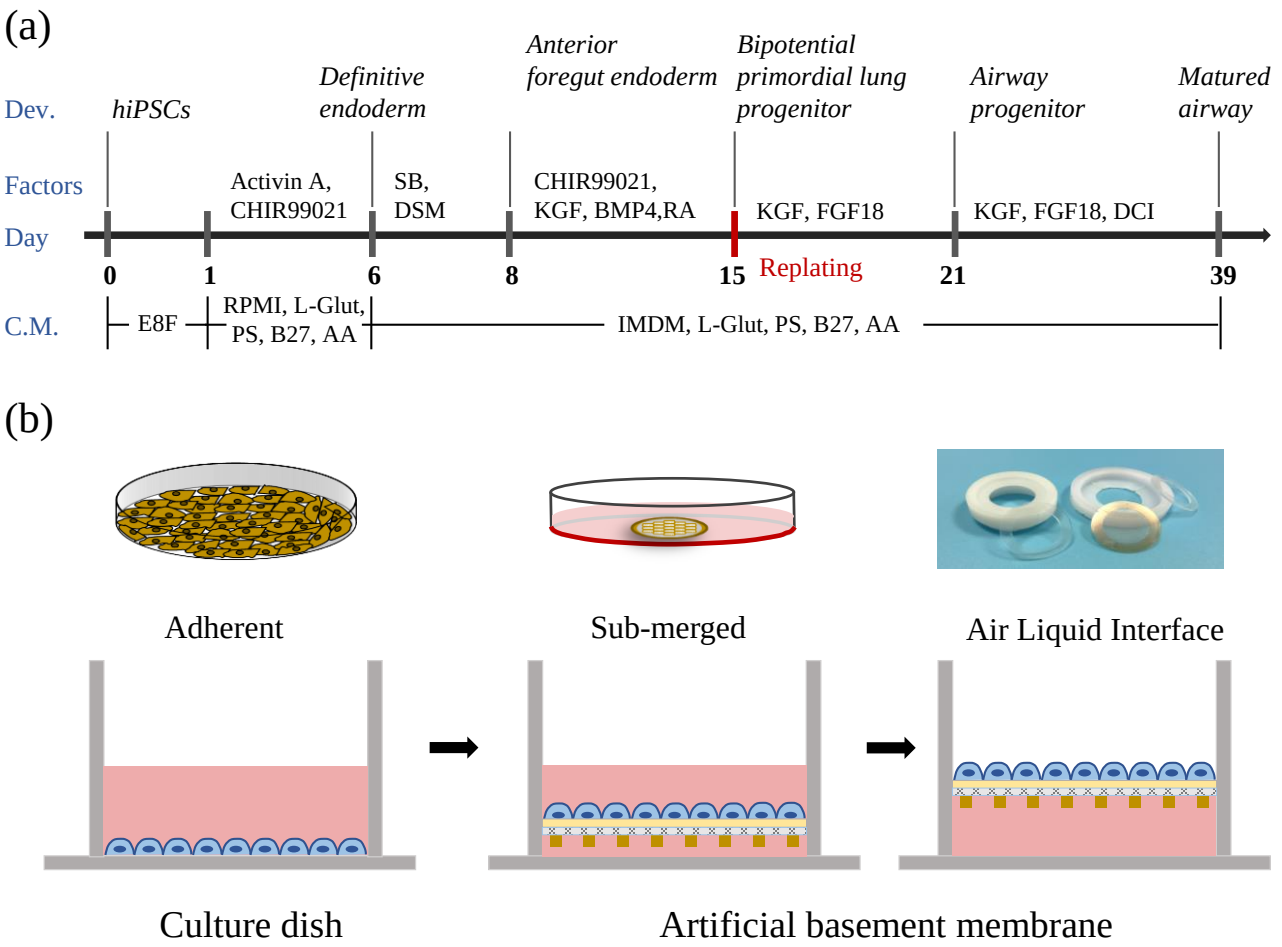
(a)
Dev.
hiPSCs
Definitive endoderm
Anterior foregut endoderm
Bipotential primordial lung progenitor
Airway progenitor
Matured airway
Factors
Activin A, CHIR99021
SB, DSM
CHIR99021, KGF, BMP4,RA
KGF, FGF18
KGF, FGF18, DCI
Day
0
1
6
8
15
Replating
21
39
C.M.
E8F
RPMI, L-Glut, PS, B27, AA
IMDM, L-Glut, PS, B27, AA
(b)
Adherent
Sub-merged
Air Liquid Interface
Culture dish
Artificial basement membrane

Figure 3

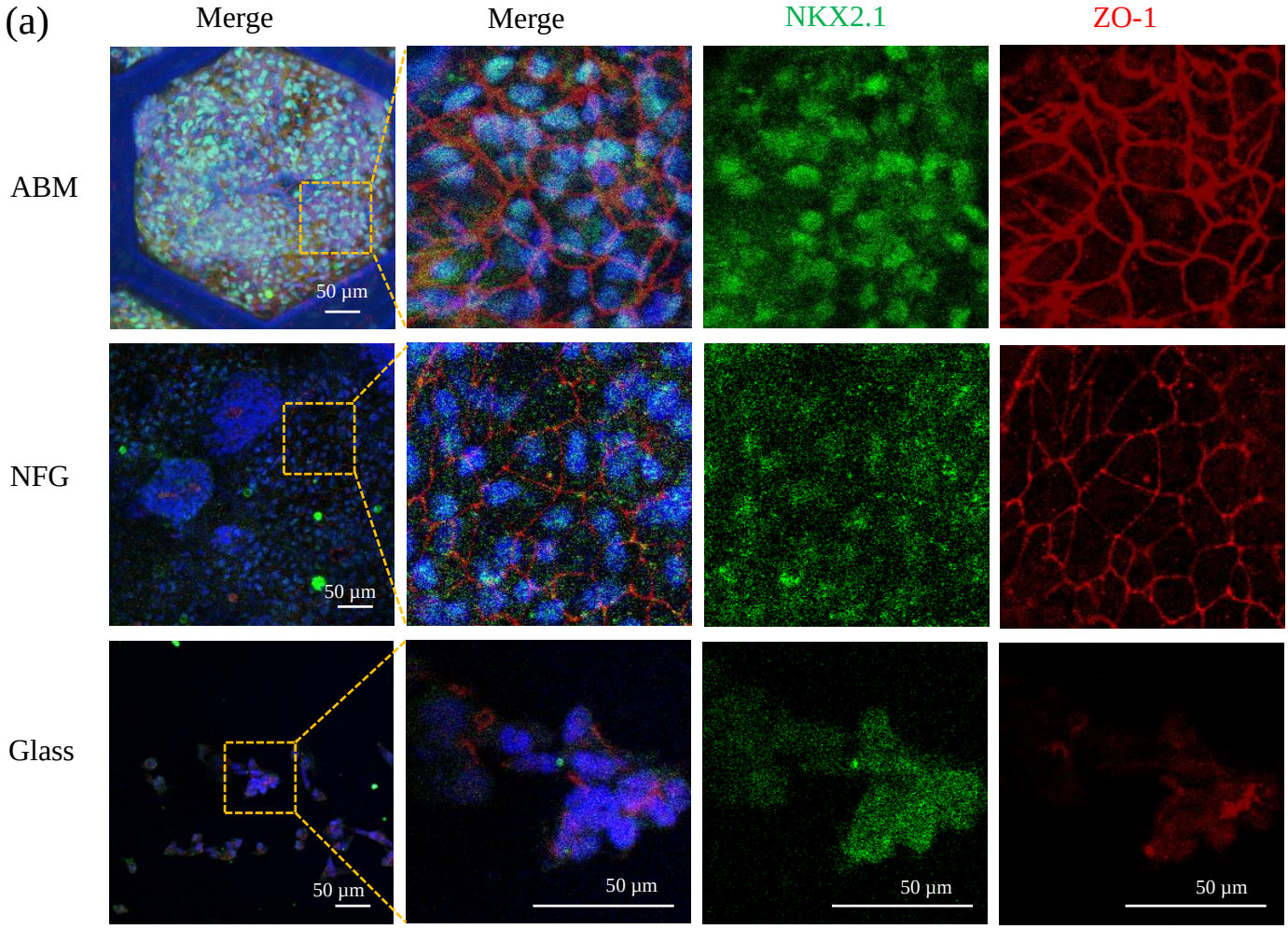
(a)
Merge
Merge
NKX2.1
ZO-1
ABM
NFG
Glass
50 μm

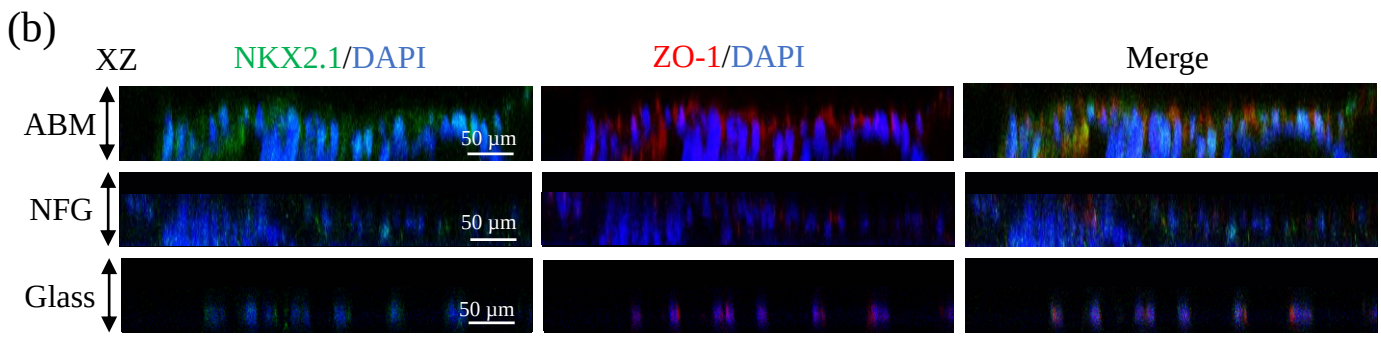
(b)
XZ
NKX2.1/DAPI
ZO-1/DAPI
Merge
ABM
NFG
Glass
50 μm

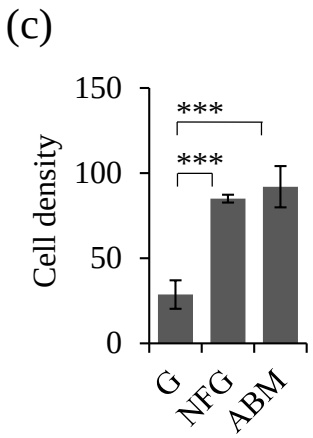
(c)
Cell density
150
100
50
0
***
***
G
NFG
ABM

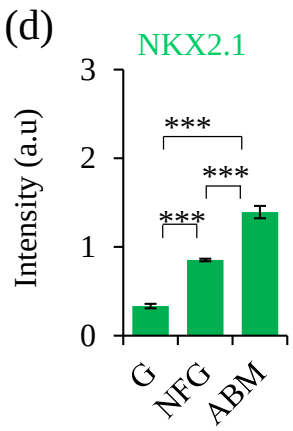
(d)
NKX2.1
Intensity (a.u)
3
2
1
0
***
***
***
G
NFG
ABM

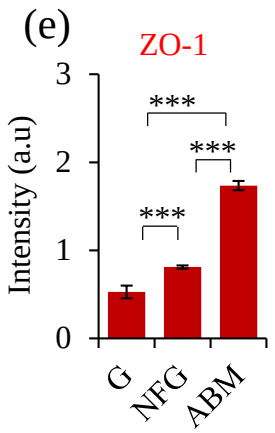
(e)
ZO-1
Intensity (a.u)
3
2
1
0
***
***
***
G
NFG
ABM

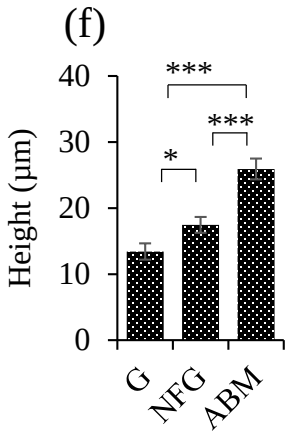
(f)
Height (μm)
40
30
20
10
0
***
*
***
G
NFG
ABM

Figure 4

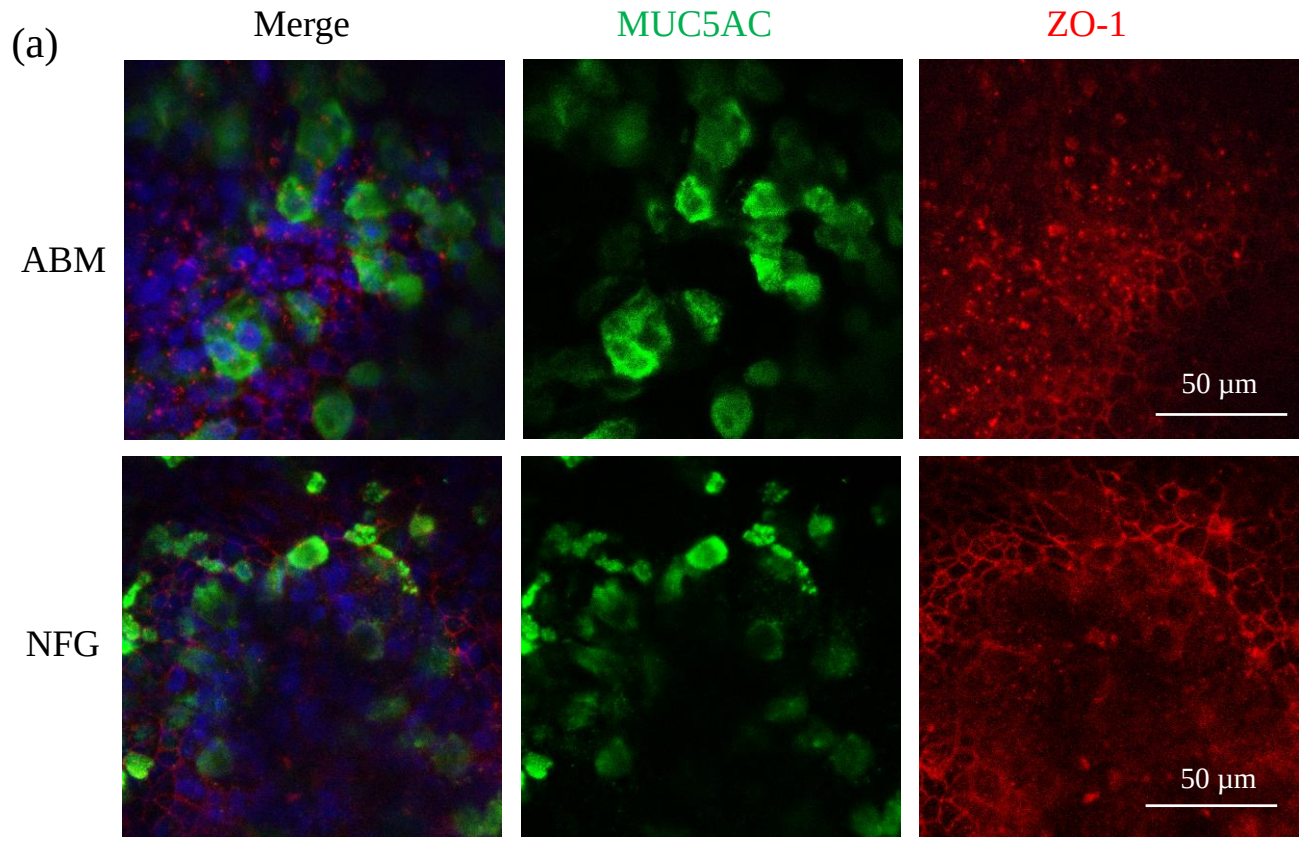
(a)
Merge
MUC5AC
ZO-1
ABM
NFG
50 μm
50 μm

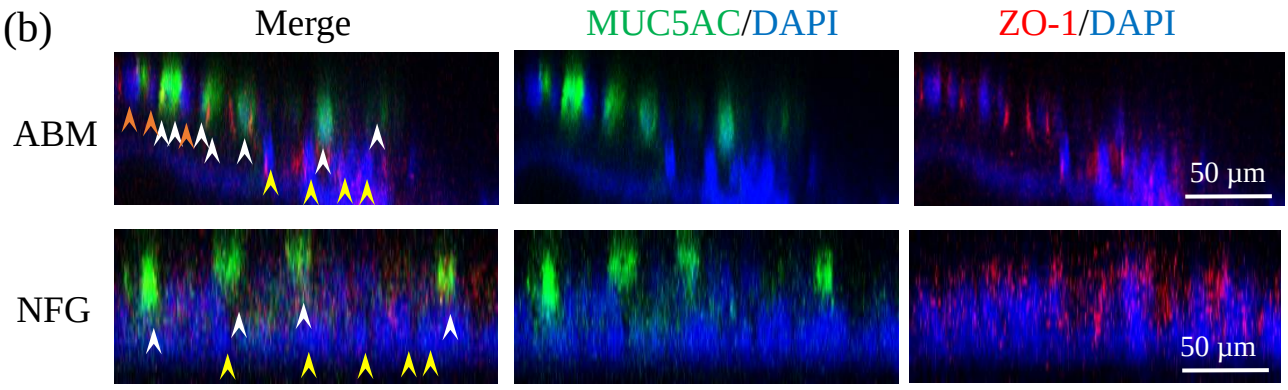
(b)
Merge
MUC5AC/DAPI
ZO-1/DAPI
ABM
NFG
50 μm
50 μm

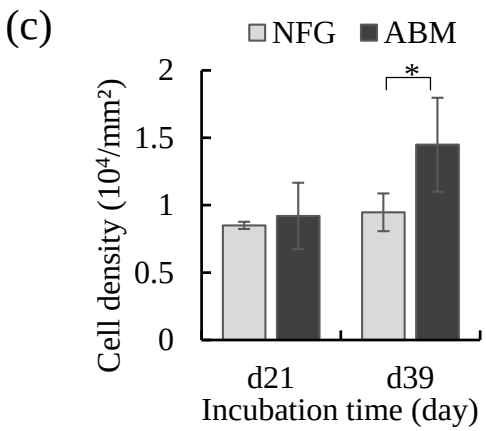
(c)
NFG
ABM
Cell density (10⁴/mm²)
2
1.5
1
0.5
0
*
d21
d39
Incubation time (day)

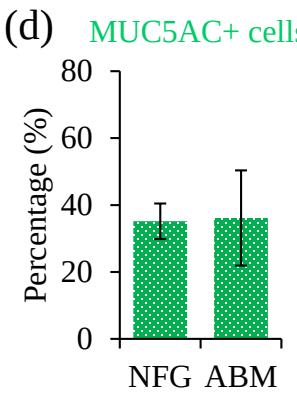
(d)
MUC5AC+ cells
Percentage (%)
80
60
40
20
0
NFG
ABM

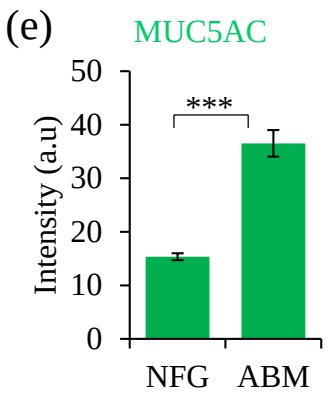
(e)
MUC5AC
Intensity (a.u)
50
40
30
20
10
0
***
NFG
ABM

Figure 5

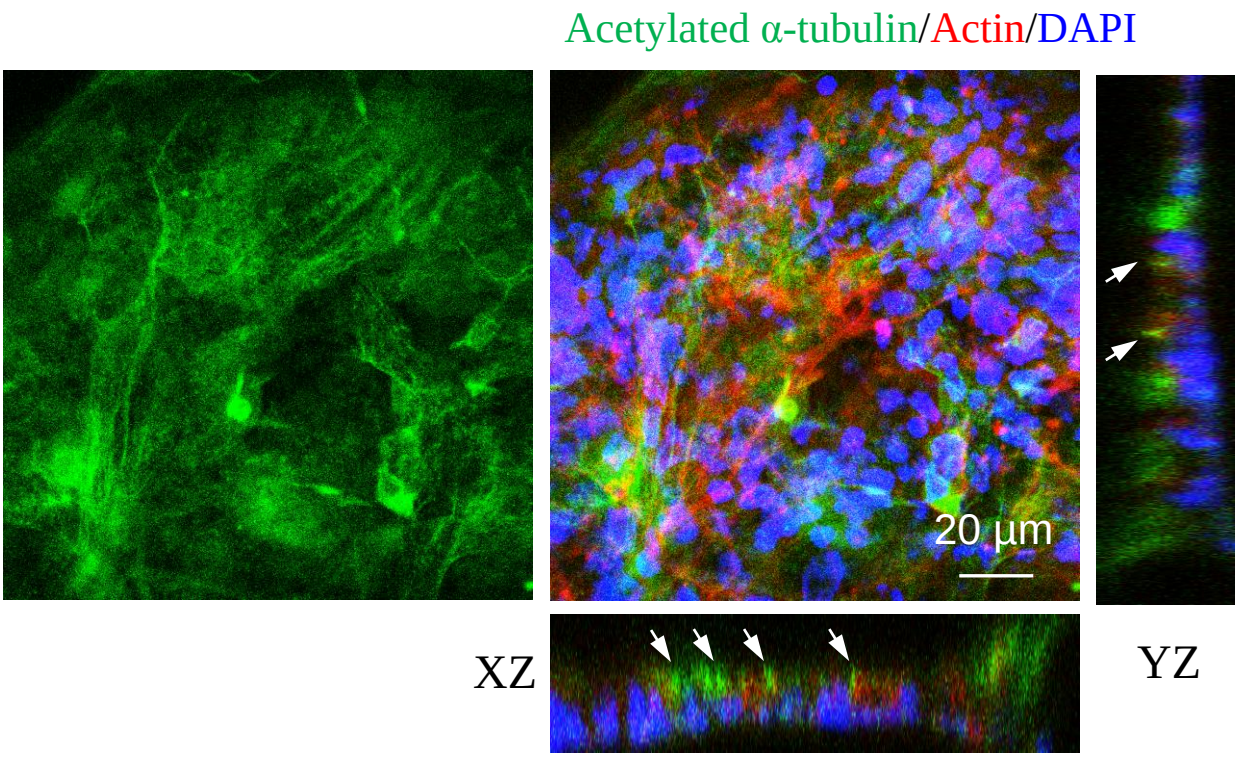

Figure 6

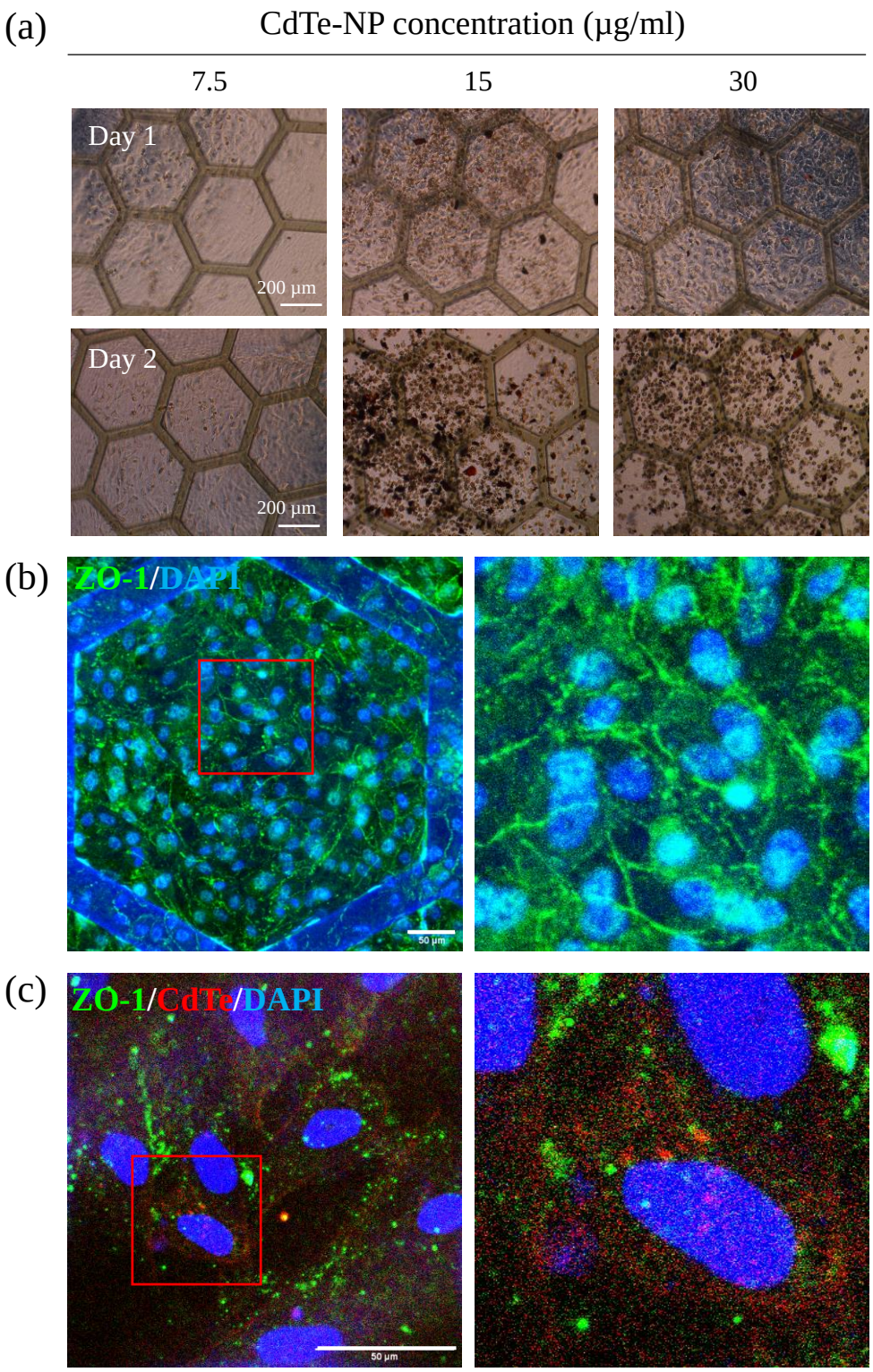
(a)
CdTe-NP concentration (μg/ml)
7.5
15
30
Day 1
200 μm
Day 2
200 μm
(b)
ZO-1/DAPI
50 μm
(c)
ZO-1/CdTe/DAPI
50 μm

Figure S1

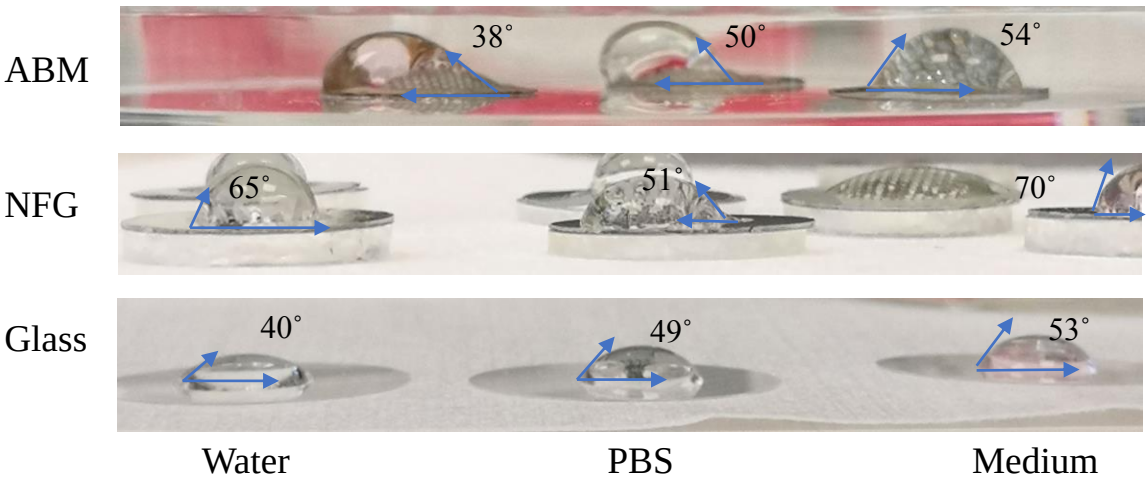

Figure S2

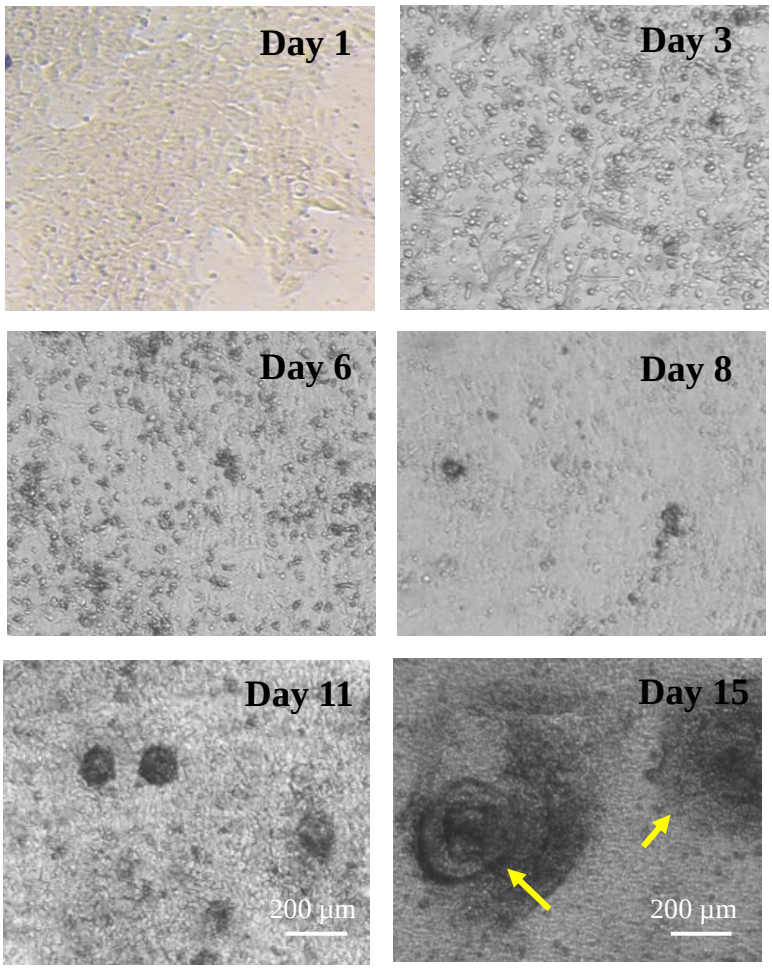

Figure S3

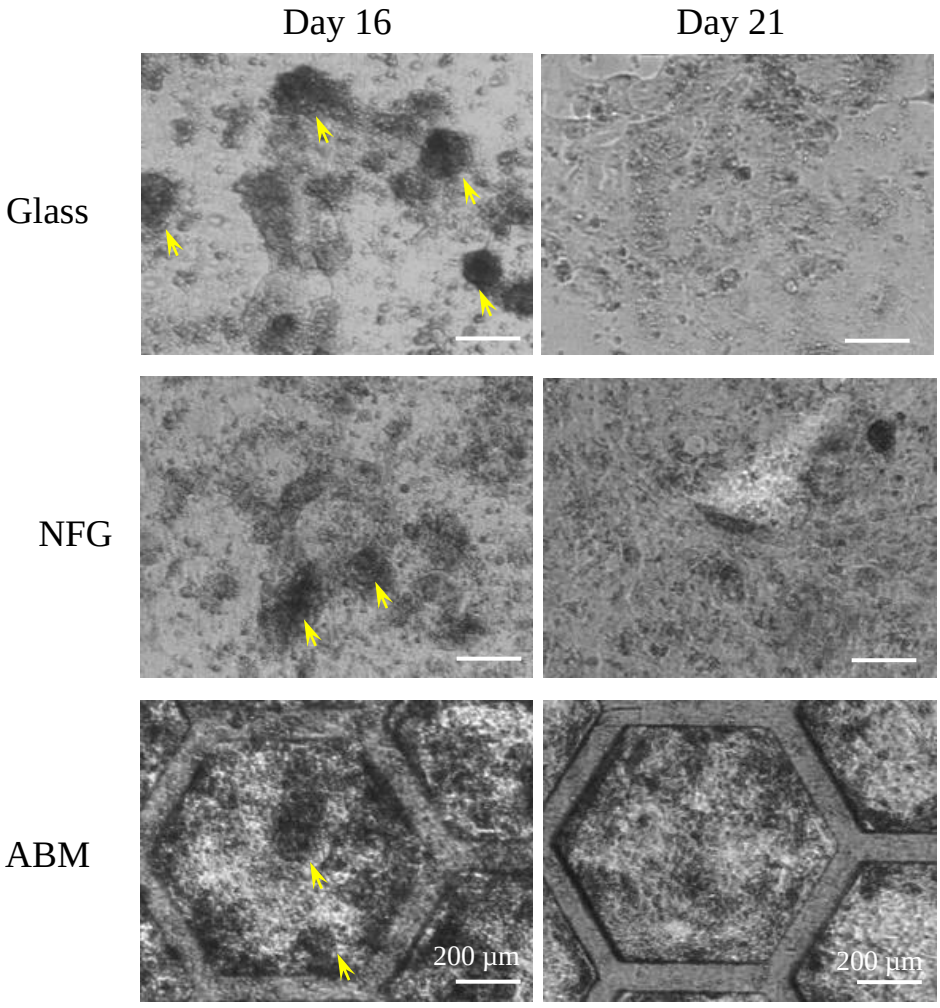

Figure S4

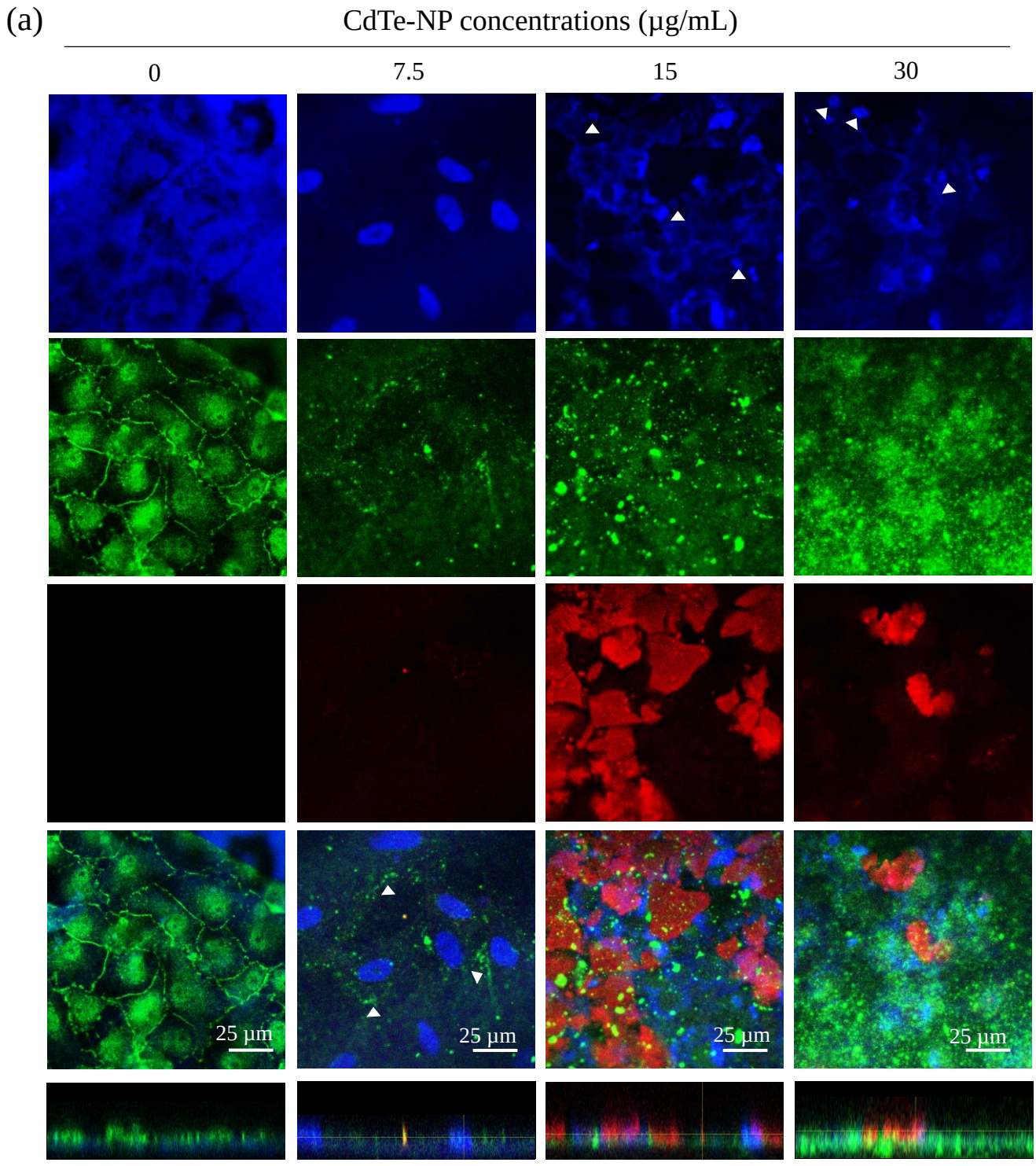
(a)
CdTe-NP concentrations (μg/mL)
0
7.5
15
30
25 μm
25 μm
25 μm
25 μm
ZO-1/CdTe/Nuclei
(b)
Nuclei size
SA (um²)
400
300
200
100
0
0 7.5 15 30
Cons. (μg/mL)
(c)
CdTe-NPs number
100
80
60
40
20
0
7.5 15 30
Cons. (μg/mL)
(d)
CdTe-NP surface area
7.5
15
30
0-50 μm²
50-100 μm²
100-1000 μm²